Ultrafast glutamate sensors resolve high-frequency release at Schaffer collateral synapses

Nordine Helassa[a,1,2], Céline D. Dürst[b,1], Catherine Coates[a], Silke Kerruth[a], Urwa Arif[a], Christian Schulze[b], J. Simon Wiegert[b,3], Michael Geeves[c], Thomas G. Oertner[b], and Katalin Török[a,4]

[a]Molecular and Clinical Sciences Research Institute, St George's, University of London, SW17 0RE London, United Kingdom; [b]Institute for Synaptic Physiology, Center for Molecular Neurobiology Hamburg, 20251 Hamburg, Germany; and [c]School of Biosciences, University of Kent, CT2 7NZ Canterbury, United Kingdom

Edited by Susan G. Amara, National Institutes of Health, Bethesda, MD, and approved April 17, 2018 (received for review November 27, 2017)

Glutamatergic synapses display a rich repertoire of plasticity mechanisms on many different time scales, involving dynamic changes in the efficacy of transmitter release as well as changes in the number and function of postsynaptic glutamate receptors. The genetically encoded glutamate sensor iGluSnFR enables visualization of glutamate release from presynaptic terminals at frequencies up to ∼10 Hz. However, to resolve glutamate dynamics during high-frequency bursts, faster indicators are required. Here, we report the development of fast (iGlu$_f$) and ultrafast (iGlu$_u$) variants with comparable brightness but increased K_d for glutamate (137 μM and 600 μM, respectively). Compared with iGluSnFR, iGlu$_u$ has a sixfold faster dissociation rate in vitro and fivefold faster kinetics in synapses. Fitting a three-state model to kinetic data, we identify the large conformational change after glutamate binding as the rate-limiting step. In rat hippocampal slice culture stimulated at 100 Hz, we find that iGlu$_u$ is sufficiently fast to resolve individual glutamate release events, revealing that glutamate is rapidly cleared from the synaptic cleft. Depression of iGlu$_u$ responses during 100-Hz trains correlates with depression of postsynaptic EPSPs, indicating that depression during high-frequency stimulation is purely presynaptic in origin. At individual boutons, the recovery from depression could be predicted from the amount of glutamate released on the second pulse (paired pulse facilitation/depression), demonstrating differential frequency-dependent filtering of spike trains at Schaffer collateral boutons.

glutamate | synaptic transmission | hippocampus | two-photon imaging

The efficacy of synaptic transmission is not constant but changes dynamically during high-frequency activity. In terms of information processing, different forms of short-term plasticity act as specific frequency filters: Facilitating synapses are most effective during high-frequency bursts, while depressing synapses preferentially transmit isolated spikes preceded by silent periods (1). Mechanistically, a number of presynaptic and postsynaptic parameters change dynamically during high-frequency activity, e.g., the number of readily releasable vesicles, presynaptic Ca^{2+} dynamics, and the properties of postsynaptic receptors, which may be altered by Ca^{2+}-activated enzymes (2, 3).

Electrophysiological analysis of short-term plasticity, by monitoring postsynaptic responses, is complicated by the fact that neurons are often connected by more than one synapse. In addition, it is not straightforward to distinguish between presynaptic and postsynaptic plasticity mechanisms. Directly measuring glutamate concentrations inside the synaptic cleft during high-frequency activity would allow isolating the dynamics of the vesicle release machinery from potential changes in glutamate receptor properties (e.g., desensitization, phosphorylation, or lateral diffusion). Early fluorescent glutamate sensors, constructed by chemical labeling of the fused glutamate binding lobes of ionotropic glutamate receptor GluA2 (termed S1S2) (4–6) and later of the bacterial periplasmic glutamate/aspartate binding protein (GluBP) (7, 8), were not suitable for quantitative single-synapse experiments due to their low dynamic range. Genetically encoded FRET-based fluorescent glutamate sensors, e.g., FLIPE, GluSnFR, and SuperGluSnFR (Fig. 1*A*), have relatively low FRET efficiency, since glutamate binding causes only a small conformational change in GluBP (9–11). A breakthrough in visualizing glutamate release in intact tissue was achieved with iGluSnFR, a single-fluorophore glutamate sensor (12). Following the concept developed for the GCaMP family of genetically encoded Ca^{2+} sensors (13), iGluSnFR was constructed from circularly permuted (cp) EGFP (14) inserted into the GluBP sequence, creating a large fragment iGlu$_l$ (residues 1–253) at the N terminus and a small fragment iGlu$_s$ (residues 254–279) at the C terminus (Fig. 1*A*). Upon glutamate binding, GluBP is reconstituted from its two fragments, pulling the cpEGFP β-barrel together, resulting in a ∼fivefold fluorescence increase. iGluSnFR is targeted for extracellular expression, like previous genetically encoded glutamate sensors, by fusion with a PDGFR peptide segment (10, 12).

iGluSnFR has high glutamate affinity and a large dynamic range but reacts relatively slowly to synaptic glutamate release with a reported decay half-time ($t_{1/2}$) of 92 ms (12). Imaging iGluSnFR in cultured hippocampal neurons during 10-Hz stimulation shows summation, which, without deconvolution, might indicate that glutamate accumulates during stimulation (15). Deconvolution of the

Significance

Excitatory synapses convert presynaptic action potentials into chemical signals that are sensed by postsynaptic glutamate receptors. To eavesdrop on synaptic transmission, genetically encoded fluorescent sensors for glutamate have been developed. However, even the best available sensors lag behind the very fast glutamate dynamics in the synaptic cleft. Here, we report the development of an ultrafast genetically encoded glutamate sensor, iGlu$_u$, which allowed us to image glutamate clearance and synaptic depression during 100-Hz spike trains. We found that only boutons showing paired-pulse facilitation were able to rapidly recover from depression. Thus, presynaptic boutons act as frequency-specific filters to transmit select features of the spike train to specific postsynaptic cells.

Author contributions: J.S.W., T.G.O., and K.T. designed research; N.H., C.D.D., C.C., U.A., and K.T. performed research; N.H., C.D.D., C.C., S.K., C.S., M.G., T.G.O., and K.T. analyzed data; and T.G.O. and K.T. wrote the paper.

The authors declare no conflict of interest.

This article is a PNAS Direct Submission.

Data deposition: The plasmids for iGlu$_f$ and iGlu$_u$ have been deposited in the Addgene database, https://www.addgene.org/75443/.

[1]N.H. and C.D.D. contributed equally to this work.

[2]Present address: Department of Cellular and Molecular Physiology, Institute of Translational Medicine, University of Liverpool, L69 3BX Liverpool, United Kingdom.

[3]Present address: Research Group Synaptic Wiring and Information Processing, Center for Molecular Neurobiology Hamburg, 20251 Hamburg, Germany.

[4]To whom correspondence should be addressed. Email: k.torok@sgul.ac.uk.

This article contains supporting information online at www.pnas.org/lookup/suppl/doi:10.1073/pnas.1720648115/-/DCSupplemental.

Published online May 7, 2018.

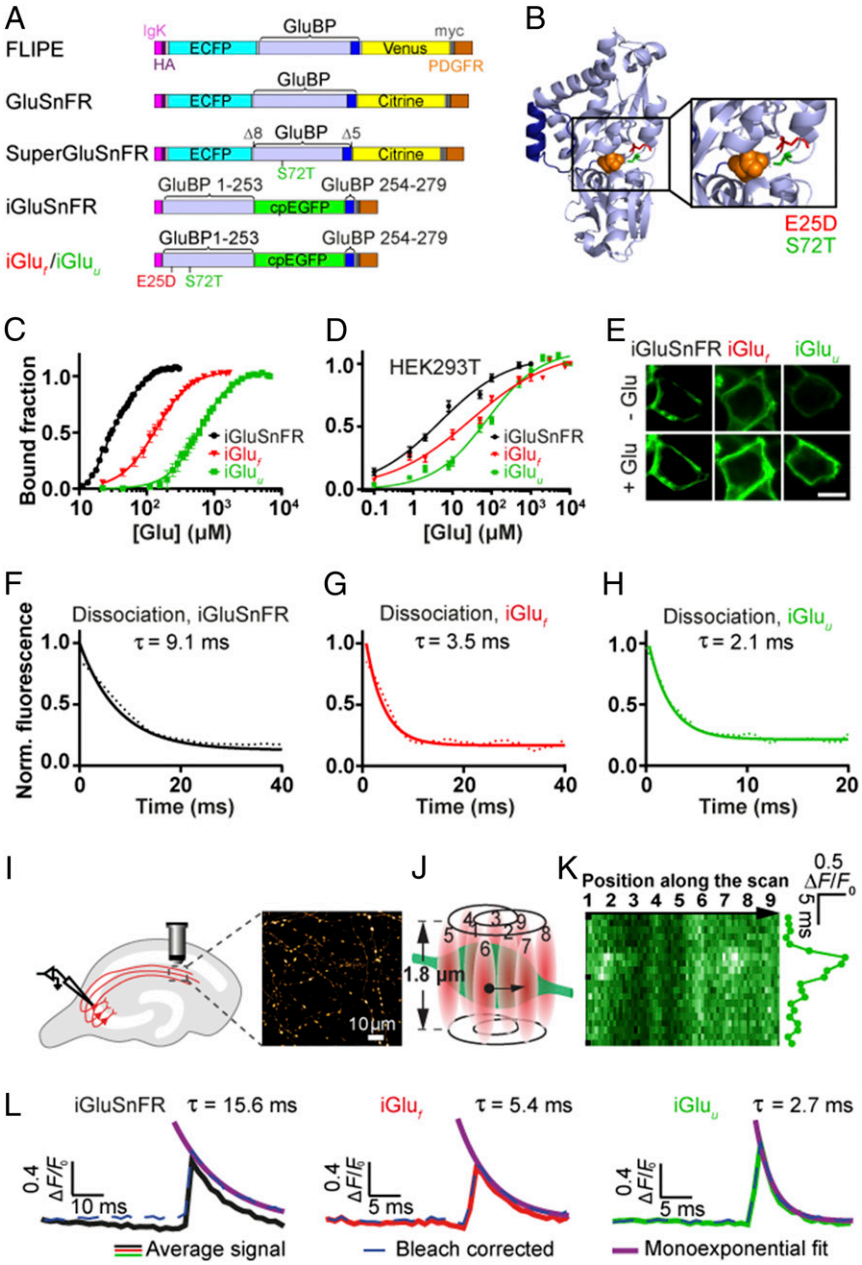

Fig. 1. Genetically encoded glutamate indicators (GEGI). (*A*) Domain structure and design of FRET- and single fluorophore-based GEGI; key: GluBP (blue), cpEGFP (green), IgG kappa secretion tag (pink), hemagglutinin (HA) tag (purple), myc tag (gray), and a PDGFR transmembrane domain (brown); GluBP 1–253 and 254–279 fragments are in light and dark blue, respectively; Δ8 aa and Δ5 aa specify deletions at the N and C terminus of GluBP introduced in GluSnFR. (*B*) Design of selected iGluSnFR variants. Crystal structure of GluBP (PDB ID code 2VHA, adapted from ref. 8). Selected mutated residues around the glutamate site are shown as red and green backbone. Bound glutamate is represented in orange space filling display. (*C*) Equilibrium glutamate binding titrations at 20 °C for iGluSnFR (black circles), iGluSnFR E25D (iGlu$_f$) (red triangles), and iGluSnFR S72T (iGlu$_u$) (green squares) in vitro. (*D*) Glutamate titrations in situ at 37 °C. iGluSnFR, iGlu$_f$, and iGlu$_u$ were expressed in HEK293T cells and titrated with glutamate. Data derived from iGluSnFR (n = 19), iGlu$_f$ (n = 41), and iGlu$_u$ (n = 33). (*E*) Representative images of HEK293T cells before glutamate addition and at saturating (1, 3, and 10 mM, respectively) glutamate. (Scale bar: 10 μm.) Glutamate dissociation kinetics of iGluSnFR (*F*), iGlu$_f$ (*G*), and iGlu$_u$ (*H*) determined by stopped-flow fluorimetry. Experimental data (dotted lines) are overlaid by curves fitted to single exponentials (solid lines). Fluorescence changes are normalized to F_{max} of 1. Imaging glutamate release from single presynaptic terminals. (*I*) Schematic representation of hippocampal slice with transfected and patch-clamped CA3 pyramidal cell. (*J*) Spiral scan intersecting site of vesicular fusion. (*K*) Zoomed-in image of single trial iGlu$_u$ response. (*L*) Decay time (τ_{off}) measurements with bleach correction (dashed lines) for individual experiments by single exponential fit for iGluSnFR (n = 13 boutons, 500 Hz sampling rate) and variants iGlu$_f$ (n = 7 boutons, 1 kHz sampling rate) and iGlu$_u$ (n = 7 boutons, 1 kHz sampling rate).

data suggests that glutamate is cleared between release events (15). Here, we introduce two fast iGluSnFR variants, iGlu$_f$ (for "fast") and iGlu$_u$ (for "ultrafast") for accurate tracking of synaptic glutamate dynamics during high-frequency transmission and identify the rate-limiting step leading to bright fluorescence upon glutamate binding. In organotypic slice cultures of rat hippocampus, iGlu$_u$ directly reports discrete synaptic glutamate release events at 100 Hz. Combining high-speed two-photon imaging and electrophysiology, we show that short-term depression of Schaffer collateral AMPA responses is fully accounted for by the depression of glutamate release. Furthermore, we show a tight correlation between paired-pulse facilitation and rapid recovery from posttetanic depression at individual boutons, suggesting that differential use of presynaptic resources (readily releasable vesicles) determines the filtering properties of CA3 pyramidal cell boutons.

Results

Affinity Variants of iGluSnFR by Binding Site Mutations. We generated six iGluSnFR variants by mutating residues coordinating glutamate or in the vicinity of the binding site (9). Two of the mutations lowered, and four increased, the K_d for glutamate. Variants in order of increasing dissociation constant (K_d) were E25A < E25R < iGluSnFR < E25D < S72T < R24K < T92A (from 19 μM to 12 mM) with Hill coefficients of 1.3–2.6 (*SI Appendix*, Fig. S1*A* and Table S1).

We selected the two variants with the fastest response kinetics, iGluSnFR E25D (termed iGlu$_f$) and iGluSnFR S72T (termed iGlu$_u$) (Fig. 1 *A* and *B*) for detailed biophysical characterization as isolated proteins and as membrane-bound glutamate sensors on HEK293T cells and pyramidal neurons. Selectivity for glutamate was determined against aspartate, glutamine, D-serine, GABA, and glycine. iGlu$_f$ and iGlu$_u$ affinities for aspartate were similar to that for glutamate, as previously reported for iGluSnFR (12), but with two- to threefold lower fluorescence enhancement. The affinity for glutamine was in the millimolar range for all three probes (*SI Appendix*, Fig. S1*B* and Table S3). D-serine, GABA, and glycine evoked no detectable response. pK_a for the glutamate-bound form was ~6.5 for iGluSnFR, iGlu$_f$, and

iGlu$_u$, whereas the apo-form showed little pH dependence, indicating a well-shielded chromophore (*SI Appendix*, Fig. S1 *C–E*). Brightness values for iGlu$_f$ and iGlu$_u$ were similar to that for iGluSnFR (*SI Appendix*, Table S2). In vitro measurements gave a K_d for glutamate of 33 μM for iGluSnFR, similar to that previously reported (12), while iGlu$_f$ and iGlu$_u$ had increased K_d values of 137 μM and 600 μM, respectively (Fig. 1*C* and *SI Appendix*, Table S1). When expressed on the membrane of HEK293T cells, K_d values for glutamate were reduced to 3.1 ± 0.3 μM for iGluSnFR, 26 ± 2 μM for iGlu$_f$, and 53 ± 4 μM for iGlu$_u$ (measured at 37 °C, Fig. 1 *D* and *E*). A similar reduction of the K_d in the cellular environment compared with that in solution was reported for iGluSnFR (12). The in situ fluorescence dynamic range ($(F_{+Glu} - F_{-Glu})/F_{-Glu}$ or $\Delta F/F_0$) was 1.0 ± 0.1 for both iGluSnFR and iGlu$_f$, but 1.7-fold larger for iGlu$_u$.

Kinetic Measurements of iGluSnFR Variants in Vitro and in Situ. Based on their large K_d values, we expected iGlu$_f$ and iGlu$_u$ to have faster glutamate release kinetics than iGluSnFR. Fluorescence measurements in a stopped-flow instrument indeed revealed faster off rates for the new variants: using the nonfluorescent high-affinity GluBP 600n (10) in excess (0.67 mM) to trap released glutamate, k_{off} values of 110 s^{-1} (τ_{off} = 9 ms), 283 s^{-1} (τ_{off} = 4 ms), and 468 s^{-1} (τ_{off} = 2 ms) were obtained for iGluSnFR, iGlu$_f$, and iGlu$_u$, respectively, at 20 °C (Fig. 1 *F–H* and *SI Appendix*, Table S4). To compare in vitro response kinetics to physiological measurements, the temperature dependencies of the off rates of iGluSnFR and the fast variants were determined. Linear Arrhenius plots were obtained between 4 °C and 34 °C (*SI Appendix*, Fig. S1 *F* and *G*). For the fast variants, values exceeding the temporal precision of our stopped-flow device were linearly extrapolated. At 34 °C, decay rates were 233 ± 3 s^{-1} for iGluSnFR (τ_{off} = 4.3 ms), 478 ± 5 s^{-1} for iGlu$_f$ (τ_{off} = 2.1 ms), and 1,481 ± 74 s^{-1} iGlu$_u$ (τ_{off} = 0.68 ms). Thus, we were able to improve iGluSnFR kinetics by a factor of 6.3.

To image glutamate dynamics in the synaptic cleft, we expressed the newly generated iGluSnFR variants in CA3 pyramidal cells in organotypic slice culture of rat hippocampus. Fluorescence was monitored at single Schaffer collateral terminals in CA1 by spiral scanning (Fig. 1 *I* and *J*) while action potentials (APs) were triggered by brief (2 ms) depolarizing current injections into the soma of the transfected CA3 neuron. A zoomed-in iGlu$_u$ example trace sampled at 1 kHz, the resolution used in all quantitative experiments with this indicator, is shown (Fig. 1*K*). The iGluSnFR response started 4.5 ± 1.6 ms (mean ± SD) after the peak of the somatic action potential, consistent with a short propagation delay between CA3 and CA1. Consistent with the stochastic nature of glutamate release, individual boutons showed different release probabilities (median p_r = 0.56, range 0.05–1.0). For kinetic analysis, boutons with high release probability and good separation between release failures and successes were selected (*SI Appendix*, Fig. S2). The measured fluorescence decay time constants (τ_{off}) were 13.8 ± 3.8 ms for iGluSnFR, 5.2 ± 2.0 ms for iGlu$_f$, and 2.6 ± 1.0 ms for iGlu$_u$ (Fig. 1 *L* and *SI Appendix*, Fig. S3). Thus, compared with iGluSnFR, synaptic responses detected by iGlu$_u$ were revealed to be faster by a factor of 5.3. Interestingly, blocking glutamate uptake with DL-threo-beta-benzyloxyaspartate (DL-TBOA, 40 μM) did not slow down the decay of iGlu$_u$ fluorescence (*SI Appendix*, Fig. S4), suggesting that after sparse activation of Schaffer collateral synapses, glutamate is rapidly cleared from the synaptic cleft by diffusion, not by active transport. The situation may be different in highly active neuropil (12, 16).

Synaptic Glutamate Dynamics During High-Frequency Stimulation. With decay kinetics of 1–2 ms, iGlu$_f$ and iGlu$_u$ are promising tools for direct tracking of synaptic glutamate during high-frequency stimulation. The response of iGluSnFR, iGlu$_f$, and iGlu$_u$ to paired-pulse stimulation (Fig. 2 and *SI Appendix*, Fig. S3) and to trains of 10 APs at 50, 67, and 100 Hz (*SI Appendix*, Fig. S5) was tested. While the responses of iGluSnFR and iGlu$_f$

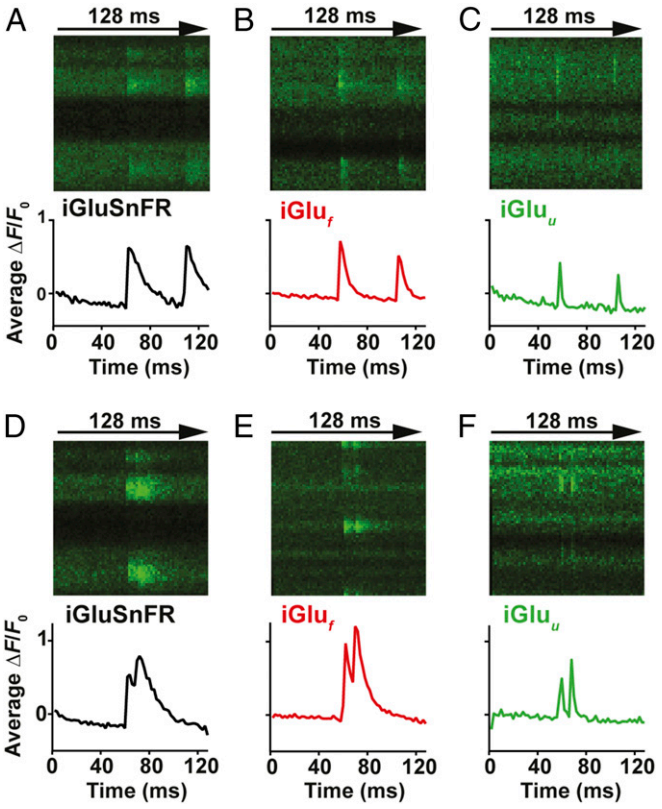

Fig. 2. Imaging glutamate release from single presynaptic terminals. Spiral line scans at 500 Hz were used to cover the entire surface of individual boutons, intersecting the release site multiple times. Averages of three to six responses of iGluSnFR (*A* and *D*), iGlu$_f$ (*B* and *E*), and iGlu$_u$-expressing (*C* and *F*) boutons stimulated by two somatic APs at 48-ms (*A–C*) and 10-ms interstimulus intervals (*D–F*).

suggested build-up of glutamate during high-frequency stimulation, iGlu$_u$ responses revealed that even at 100-Hz stimulation, glutamate was completely cleared from the synaptic cleft between APs (Fig. 2*F* and *SI Appendix*, Fig. S5*I*). Interestingly, the amplitudes of synaptic fluorescence signals ($\Delta F/F_0$) were similar for all three indicators, suggesting that the on rate, not the overall affinity, determined the number of glutamate-bound indicator molecules in the synaptic cleft.

Excitatory postsynaptic potentials (EPSPs) in CA1 become strongly depressed during high-frequency stimulation (17). We were interested whether EPSP depression during 100-Hz stimulation could be fully accounted for by depression of glutamate release from presynaptic boutons. In paired recordings from connected CA3-CA1 pyramidal cells, we triggered APs in the CA3 cell by brief current injections while monitoring postsynaptic potentials (EPSPs) in the CA1 cell. The protocol consisted of a short high-frequency burst (10 APs at 100 Hz) followed by a single AP 500 ms after the burst to probe recovery of synaptic function (18). We repeated the protocol up to 100 times at 0.1 Hz and averaged the recorded traces (Fig. 3 *A–C*). As expected, connected CA3-CA1 pyramidal cell pairs showed strong depression during the high-frequency train. The response to the recovery test pulse (#11) was not significantly different from the first EPSP in the train, indicating full recovery of synaptic function. To investigate depression and recovery of glutamate release, we evaluated iGlu$_u$ signals during identical stimulation (Fig. 3 *D* and *E*). Due to the extremely fast kinetics of the indicator, deconvolution of the fluorescence time course was not necessary: We read the peak amplitudes during the 100-Hz train directly from the averaged fluorescence time course

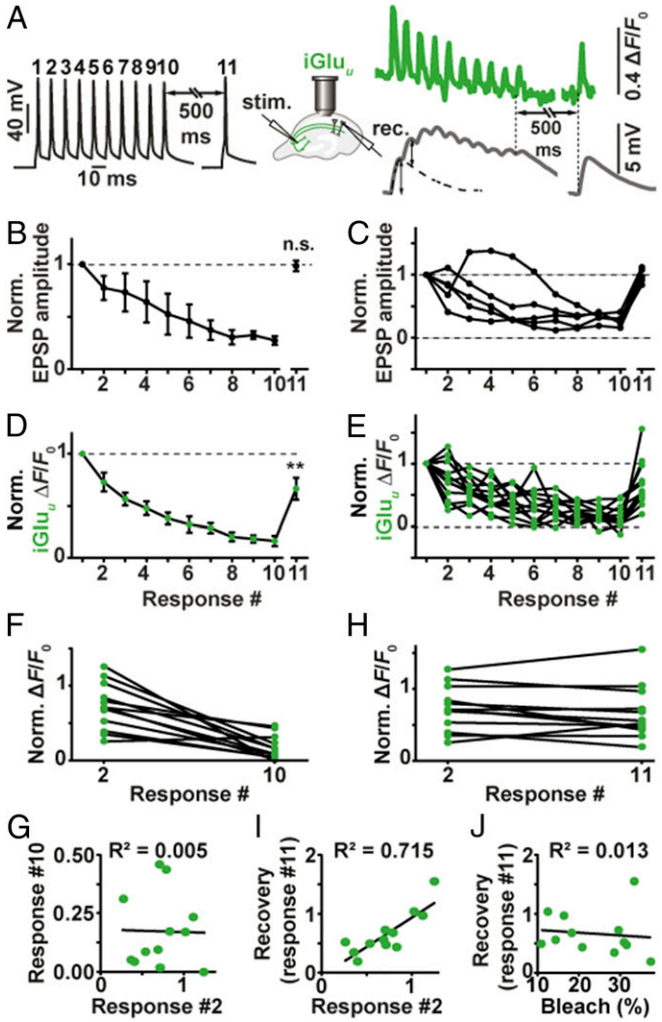

Fig. 3. Depression and recovery of synaptic transmission during 100-Hz trains. (*A*) Example of patch-clamp recording from a connected pair of CA3-CA1 pyramidal cells. Black trace: induced APs in CA1 pyramidal cell, 100-Hz train and single AP. Gray trace: EPSPs in CA1 pyramidal cell (average of 50 sweeps). The single AP response (*Right*) was used to extract EPSP amplitudes from the burst response (dotted line). Green trace: average of 10 sweeps of single-bouton iGlu$_u$ responses to identical stimulation. (*B*) EPSPs (deconvolved amplitudes) show strong depression during the 100-Hz train, followed by full recovery 500 ms later ($n = 5$ CA3-CA1 pairs); two-tailed Student's *t* test comparing EPSP #1 and EPSP #11. (*C*) Individual paired recordings show consistent depression (response #10) and recovery (response #11). (*D*) Glutamate release shows strong depression during the 100-Hz train and partial recovery 500 ms later ($n = 12$ boutons, eight cells); two-tailed Student's *t* test comparing response #1 and response #11 (*P* value: 0.0034). (*E*) Individual Schaffer collateral boutons show large variability in response #2 and in recovery response (#11) (*F* and *G*) responses by iGlu$_u$ to the second AP (paired-pulse facilitation/depression) were not correlated with total depression (response #10 normalized to response #1). (*H* and *I*) iGlu$_u$ responses to the second AP (response #2 normalized to response #1) were highly correlated with recovery after 500 ms (response #11 normalized to response #1). (*J*) Recovery was independent of indicator bleach ($F_{0,\ \text{response #11}}/F_{0,\ \text{response #1}}$).

(average of 10 individual trials sampled at 1 kHz). Glutamate release decreased during the train with a time course that matched EPSP depression (Fig. 3*D*). This result points to a purely presynaptic origin of depression, which is consistent with AMPA receptors rapidly recovering from desensitization after each release event (recovery = 5 ms; ref. 19). However, glutamate release 500 ms after the tetanus was still significantly depressed (two-tailed Student's test, *P* value: 0.0034) while AMPA receptor currents were not. This discrepancy suggests that the response of AMPA receptors to cleft glutamate was in fact potentiated 500 ms after the high-frequency train, compensating for the reduced output of Schaffer collateral boutons.

Paired-Pulse Facilitation Correlates with Rapid Recovery from Depression. The rapid kinetics of iGlu$_u$ allowed us to analyze frequency filtering at individual boutons. On the second AP, boutons showed a wide range of facilitated (3 of 12 boutons) or depressed responses (9 of 12 boutons, Fig. 3*E*). The response to the 10th AP was strongly depressed in all boutons (16% of response amplitude to first AP), with no correlation between the second and the 10th response ($R^2 = 0.005$, Fig. 3 *F* and *G*). Interestingly, a highly significant correlation was observed between the response to the second AP and the recovery response 500 ms after the high-frequency train ($R^2 = 0.715$, Fig. 3 *H* and *I*). In contrast, we found no correlation between the amount of bleaching in individual experiments (F_0(pre-11th pulse)/F_0(pre-first pulse) and the amplitude of the recovery response $((\Delta F/F_0)_{11\text{th pulse}}/(\Delta F/F_0)_{\text{first pulse}})$, indicating that poor recovery was not caused by excessive bleaching or dilution of indicator molecules (Fig. 3*J*). Thus, synapses that showed pronounced paired-pulse facilitation were also able to recover rapidly from depression, both of which is indicative of a low utilization of presynaptic resources (18). Such boutons are optimized for the transmission of high-frequency activity (spike bursts). In contrast, boutons that showed paired-pulse depression were still depressed 500 ms after the high-frequency train. These boutons act as low-pass filters: They preferentially transmit isolated APs preceded by a silent period.

Response Kinetics of iGluSnFR and Variants iGlu$_f$ and iGlu$_u$ Are Based on the Rate of Structural Change. Finally, we investigated the response mechanism of iGluSnFR and its fast variants using fluorescence stopped flow with millisecond time resolution. In association kinetic experiments (20 °C), the fluorescence response rates (k_{obs}) showed hyperbolic glutamate concentration dependence, approaching saturating rates of 643 s^{-1} and 1,240 s^{-1} for iGluSnFR and iGlu$_f$, respectively (Fig. 4 *A*–*D*). For iGlu$_u$, in contrast, k_{obs} was found to be concentration-independent at 604 s^{-1} (Fig. 4 *E* and *F*). We considered two different reaction pathways to explain our kinetic data (Fig. 4*G*). iGluSnFR is represented as a complex of the large fragment of the GluBP domain (GluBP 1–253, iGlu$_l$), N-terminally flanking cpEGFP and of the C-terminally fused small GluBP fragment (GluBP 254–279, iGlu$_s$). The term iGlu$_l$ ~ iGlu$_s$ indicates that the large GluBP fragment iGlu$_l$ and the small fragment iGlu$_s$ are within one molecule, albeit separated by the interjecting cpEGFP. In *SI Appendix*, Scheme 1, the binding of glutamate to iGlu$_l$ in iGlu$_l$ ~ iGlu$_s$ is the primary step (no change in fluorescence). Glutamate binding is followed by a conformational change induced by the reattachment of iGlu$_s$ to Glu-bound iGlu$_l$, resulting in the highly fluorescent Glu.iGlu$_c$* complex (rate-limiting step). According to *SI Appendix*, Scheme 1, the hyperbolic dependence of the observed rate k_{obs} on the glutamate concentration [Glu] has the intercept of the *y* axis at k_{-2} (*SI Appendix*, *Kinetic Theory* and Eq. 7). At low [Glu], the initial linear slope gives $k_{+2}K_1$. At high [Glu], k_{obs} tends to $k_{+2} + k_{-2}$. Although k_{obs} for iGlu$_u$ appears essentially concentration independent, its kinetics is consistent with *SI Appendix*, Scheme 1, with $k_{+2} + k_{-2}$ having a similar value to k_{-2} (*SI Appendix*, Table S5).

In the alternative pathway (*SI Appendix*, Scheme 2), the reattachment of iGlu$_s$ to iGlu$_l$ occurs without prior binding of glutamate. Therefore, iGlu$_l$ ~ iGlu$_s$ with the GluBP fragments separated and complete GluBP domain (iGlu$_c$*) are in equilibrium. The conformational change that represents the reattachment of the two GluBP fragments is expected to generate a fluorescent state of cpEGFP. However, the equilibrium is likely to be strongly shifted to the separated, nonfluorescent state (iGlu$_l$ ~ iGlu$_s$). Assuming that this equilibrium is fast and glutamate binding stabilizes the fluorescent state, at low [Glu], a linear dependence of k_{obs} on [Glu] is predicted with a slope

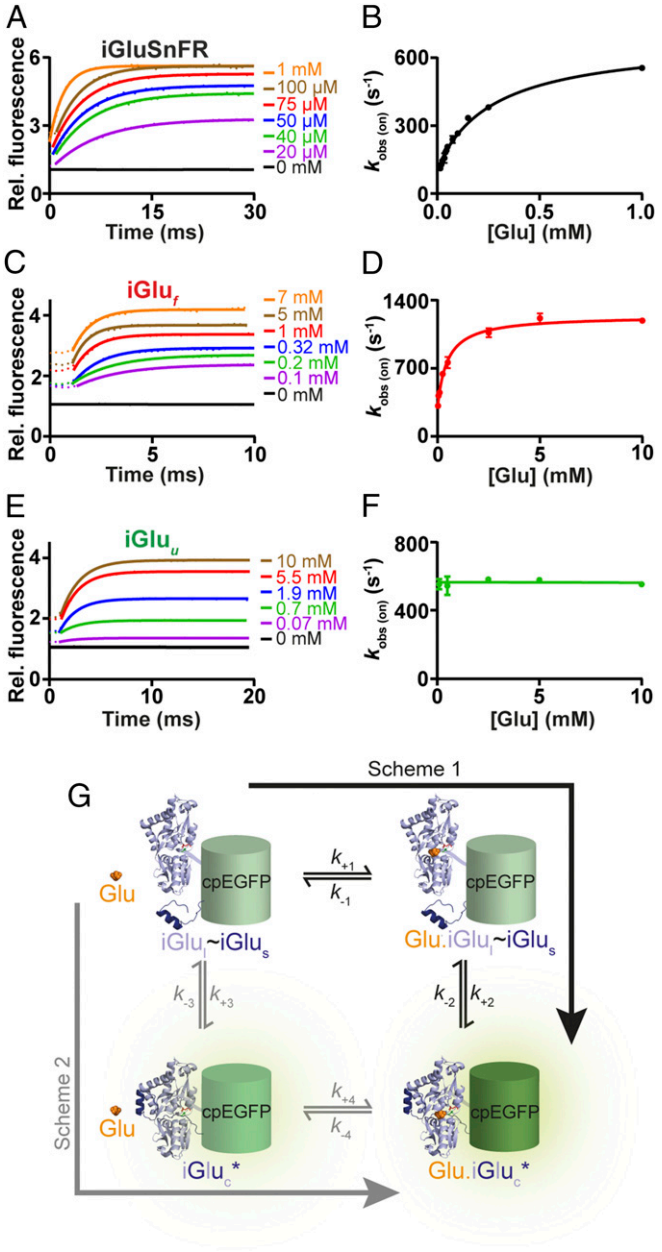

Fig. 4. Kinetics of glutamate binding by iGluSnFR variants (20 °C). (*A*, *C*, and *E*) Glutamate association kinetics of iGluSnFR, $iGlu_f$, and $iGlu_u$, respectively. Stopped-flow records of iGluSnFR, $iGlu_f$, and $iGlu_u$ reacting with the indicated concentrations of glutamate. Experimental data (dotted lines) are overlaid with curves fitted to single exponentials (solid lines). (*B*, *D*, and *F*) Plot of observed association rates, $k_{obs(on)}$ of iGluSnFR, $iGlu_f$, and $iGlu_u$ as a function of glutamate concentration. (*G*) Cartoon diagram depicting the putative molecular transitions of iGluSnFR and its fast variants to the fluorescent state. Key: cpEGFP (green), GluBP 1–253 ($iGlu_l$) (light blue) and 254–279 ($iGlu_s$) (dark blue) fragments, glutamate (orange).

of $K_3k_{+4}/(1 + K_3)$ and an intercept of the y axis at k_{-2} (*SI Appendix*, *Kinetic Theory* and Eq. **15**). Although at low [Glu] monoexponential fluorescence changes are expected, as [Glu] increases, the concentration of $iGlu_c$* cannot be assumed to be at steady state and slow isomerization will limit k_{obs}, in a similar pattern to that for *SI Appendix*, Scheme 1. Thus, at high [Glu], even if $iGlu_c$* and Glu.$iGlu_c$* have equal relative fluorescence intensities, biphasic fluorescence changes would be expected for the association reactions. As all of the reactions studied here for the three variants had a single exponential appearance, we can exclude *SI Appendix*, Scheme 2 as a possible reaction pathway. In conclusion, *SI Appendix*, Scheme 1 provides an excellent fit to our measurements (*SI Appendix*, Table S5), pointing to "Venus fly-trap" closure by glutamate binding as a required first step for the conformational change that increases iGluSnFR fluorescence.

Discussion

The development of iGluSnFR was a breakthrough in fluorescent glutamate sensors toward investigating neurotransmission in living organisms (20). Here, we describe how to overcome one of the key limitations of iGluSnFR, its slow response kinetics, and use the ultrafast variant $iGlu_u$ to investigate synaptic transmission and frequency filtering at individual Schaffer collateral boutons. For all tested variants, synaptic off kinetics was slower by a factor of 2.5–3.8 compared with temperature-matched in vitro measurements on isolated protein. This is consistent with the much higher affinities of HEK293T cell-expressed glutamate sensors compared with soluble protein. These systematic differences, also noted in the original characterization of iGluSnFR (12), may be attributed to the tethering of the molecule to a membrane anchor, slowing down conformational changes compared with free-floating sensor molecules. Nevertheless, the relative differences in affinity and kinetics of the new versions compared with iGluSnFR were preserved in vitro and in situ. The on and off rates of $iGlu_u$ are greater (two- and five- to sixfold, respectively) compared with iGluSnFR. Interestingly, $iGlu_u$ was a faster reporter in the hippocampal slice than $iGlu_f$, although the latter has a faster limiting on rate. $iGlu_u$ may be put at an advantage over $iGlu_f$ by its concentration-independent response kinetics. It must be noted that the kinetics of iGluSnFR-type indicators are ultimately limited by the structural change that reconstitutes the fluorescent complex, similar to calcium-sensing GCaMPs. The constraints of the mechanism with regard to the onset of fluorescence suggest that it cannot be engineered to resolve submillisecond glutamate dynamics. To achieve microsecond response times, it might be necessary to develop hybrid glutamate indicators using synthetic dyes.

Synaptic $iGlu_u$ imaging revealed complete clearance of glutamate between release events even at 100-Hz stimulation frequency. The first attempts to estimate the time course of synaptic glutamate transients were based on the decay of NMDA receptor responses in primary cell culture: Kinetic analysis of the displacement of a competitive NMDA receptor antagonist suggested glutamate clearance with $\tau = 1.2$ ms (21). More recent studies using computational modeling and fluorescence anisotropy imaging in tissue suggest that it is closer to 100 μs (22, 23). Thus, due to the intrinsic kinetic limits of the iGluSnFR mechanism, even $iGlu_u$ cannot resolve the true dynamics of free glutamate in the synaptic cleft. Moreover, our spatiotemporal resolution is limited by scanning, although in most experiments, the spiral scan line intersected the release site two or more times and, thus, effectively increased temporal sampling of cleft glutamate by the same factor (e.g., from 1 to 2 kHz). In our analysis, we binned all measurements (pixels) of a scan line into a single time point (1 ms), potentially undersampling the sharp peak of $iGlu_u$ signals (*SI Appendix*, Fig. S6). For experiments where the peak amplitude of $iGlu_u$ signals is of critical importance, temporal sampling could be improved by assigning a time value to every pixel of the spiral scan line before analysis (*SI Appendix*, Fig. S2). What we can say with confidence is that accumulation of glutamate in the synaptic cleft does not contribute to short-term plasticity at Schaffer collateral synapses.

Glutamate release showed strong depression during 100-Hz firing, in line with the expected depletion of release-ready vesicles. As we controlled the generation of every action potential by somatic current injections, we can exclude decreased afferent excitability as a source of depression in these experiments (17). AMPA receptor currents during 100-Hz firing did not show more rundown than $iGlu_u$ responses, suggesting that AMPA receptor desensitization did not play a major role in the decrease of synaptic efficacy during the train. Paradoxically, AMPA

responses were fully recovered 500 ms after the train while the $iGlu_u$ response was still significantly depressed. The most parsimonious explanation is a long-lasting depression of glutamate release. There are alternative scenarios that could explain smaller $iGlu_u$ responses on the 11th pulse, e.g., indicator molecules retrieved into endosomal structures during endocytosis, or accumulation of indicator in a (hypothetical) desensitized state. In these scenarios, facilitating boutons, which experience more exocytosis and endocytosis and $iGlu_u$ activation during the train, would be expected to show smaller responses at the 11th pulse. However, we found a strong correlation in the opposite direction (Fig. 3*I*), making these scenarios less likely.

As response amplitudes (40–120% $\Delta F/F_0$) were typically less than half of the maximum change in fluorescence we determined for the three indicators (*SI Appendix*, Table S3), we did not correct for the nonlinearity of the iGluSnFR variants (Fig. 1*C*). To determine the absolute (or "peak") glutamate concentration in the synaptic cleft, however, indicator saturation and undersampling would have to be taken into account.

The full recovery of the AMPA response points to an unexpected increase in sensitivity of the postsynaptic compartment to glutamate. By association with different auxiliary proteins and other scaffold-related mechanisms, the density and open probability of postsynaptic glutamate receptors can quickly change (24, 25). In hippocampal slice cultures, posttetanic potentiation is well established and requires the activity of protein kinase C (26). Thus, it is possible that elevated Ca^{2+} levels in the spine during our high-frequency protocol enhanced AMPA receptor currents by a number of mechanisms, compensating for the reduced glutamate release 500 ms after the tetanus.

The surprisingly tight correlation between paired-pulse facilitation and rapid recovery from depression at individual boutons provides direct evidence that differential use of presynaptic resources determines the neural code between pyramidal cells (1, 18). Using Schaffer collateral synapses as an example, we show that $iGlu_u$ is a useful tool for a mechanistic analysis of high-frequency synaptic transmission, interrogating presynaptic function independently of postsynaptic transmitter receptors.

Methods

We provide a detailed description of the methods, data analysis, and kinetic modeling in *SI Appendix*.

Materials. pCMV(MinDis).iGluSnFR and pRSET FLIPE-600n plasmids were a gift from Loren Looger, Janelia Research Campus, Howard Hughes Medical Institute, Ashburn, VA (Addgene plasmid 41732) and Wolf Frommer, Heinrich Heine University, Düsseldorf, Germany (Addgene plasmid 13537), respectively. Site-directed mutagenesis was carried out following the QuikChange II XL protocol (Agilent Technologies).

Fluorescence Spectroscopies. Glutamate association and dissociation kinetic experiments of iGluSnFR proteins were carried out on a Hi-Tech Scientific SF-61DX2 stopped-flow system equipped with a temperature manifold (27). Fluorescence spectra and equilibrium glutamate titrations were recorded on a Fluorolog3 (Horiba Scientific).

In Situ Glutamate Titration. HEK293T cells were cultured on 24-well glass bottom plates in DMEM containing nonessential amino acids (Life Technologies), 10% heat inactivated FBS (Life Technologies), and penicillin/streptomycin (100 U/mL, 100 mg/mL, respectively), at 37 °C in an atmosphere of 5% CO_2. Cells were allowed 24 h to adhere before transfection with Lipofectamine 2000 (Invitrogen). Cells were examined at 37 °C (OKO laboratory incubation chamber) with a 3i Marianas spinning-disk confocal microscope equipped with a Zeiss AxioObserver Z1, a 40×/N.A. 1.3 oil immersion objective and a 3i Laserstack as excitation light source (488 nm).

Synaptic Measurements. Organotypic hippocampal slices (400 μm) were prepared from male Wistar rats at postnatal day 5 as described (28). iGluSnFR and variant plasmids were electroporated into 2–3 CA3 pyramidal cells at 40 ng/μL (iGluSnFR) or 50 ng/μL ($iGlu_f$, $iGlu_u$) together with tdimer2 (20 ng/μL), a cytoplasmic red fluorescent protein (29). Two to four days after electroporation (at 14–30 days in vitro), slice cultures were placed in the recording chamber of a two-photon microscope and superfused with artificial cerebrospinal fluid. Whole-cell recordings from a transfected CA3 pyramidal cell were made with a Multiclamp 700B amplifier (Molecular Devices). Red and green fluorescence was detected through the objective (LUMPLFLN 60XW, 60×, N.A. 1.0; Olympus) and through the oil immersion condenser (N.A. 1.4; Olympus) using two pairs of photomultiplier tubes (H7422P-40SEL, Hamamatsu).

ACKNOWLEDGMENTS. We thank Dr. Zoltan Ujfalusi (University of Kent) for assistance with stopped-flow experiments, Iris Ohmert for the preparation of organotypic cultures, and Dr. David Trentham for comments on the manuscript. Use of The Institute of Translational Medicine, University of Liverpool Imaging Facility is gratefully acknowledged. This project was supported by Wellcome Trust Grant 094385/Z/10/Z (to K.T.); Biotechnology and Biological Sciences Research Council Grant BB/M02556X/1 (to K.T.); German Research Foundation Grants SPP 1665, SFB 936, FOR 2419 (to T.G.O.), SPP 1926, and FOR 2419 (to J.S.W.); and European Research Council Grant ERC-2016-StG 714762 (to J.S.W.).

1. Markram H, Wang Y, Tsodyks M (1998) Differential signaling via the same axon of neocortical pyramidal neurons. *Proc Natl Acad Sci USA* 95:5323–5328.
2. Regehr WG (2012) Short-term presynaptic plasticity. *Cold Spring Harb Perspect Biol* 4:a005702.
3. Jenkins MA, Traynelis SF (2012) PKC phosphorylates GluA1-Ser831 to enhance AMPA receptor conductance. *Channels (Austin)* 6:60–64.
4. Best SL, Török K (2005) Development of a fluorescent glutamate binding protein. *Biophys J* 88:46a.
5. Chen GQ, Gouaux E (1997) Overexpression of a glutamate receptor (GluR2) ligand binding domain in Escherichia coli: Application of a novel protein folding screen. *Proc Natl Acad Sci USA* 94:13431–13436.
6. Kuusinen A, Arvola M, Keinänen K (1995) Molecular dissection of the agonist binding site of an AMPA receptor. *EMBO J* 14:6327–6332.
7. de Lorimier RM, et al. (2002) Construction of a fluorescent biosensor family. *Protein Sci* 11:2655–2675.
8. Hu Y, et al. (2008) Crystal structure of a glutamate/aspartate binding protein complexed with a glutamate molecule: Structural basis of ligand specificity at atomic resolution. *J Mol Biol* 382:99–111.
9. Hires SA, Zhu Y, Tsien RY (2008) Optical measurement of synaptic glutamate spillover and reuptake by linker optimized glutamate-sensitive fluorescent reporters. *Proc Natl Acad Sci USA* 105:4411–4416.
10. Okumoto S, et al. (2005) Detection of glutamate release from neurons by genetically encoded surface-displayed FRET nanosensors. *Proc Natl Acad Sci USA* 102:8740–8745.
11. Tsien RY (2005) Building and breeding molecules to spy on cells and tumors. *FEBS Lett* 579:927–932.
12. Marvin JS, et al. (2013) An optimized fluorescent probe for visualizing glutamate neurotransmission. *Nat Methods* 10:162–170.
13. Nakai J, Ohkura M, Imoto K (2001) A high signal-to-noise Ca(2+) probe composed of a single green fluorescent protein. *Nat Biotechnol* 19:137–141.
14. Baird GS, Zacharias DA, Tsien RY (1999) Circular permutation and receptor insertion within green fluorescent proteins. *Proc Natl Acad Sci USA* 96:11241–11246.
15. Taschenberger H, Woehler A, Neher E (2016) Superpriming of synaptic vesicles as a common basis for intersynapse variability and modulation of synaptic strength. *Proc Natl Acad Sci USA* 113:E4548–E4557.
16. Zheng K, Rusakov DA (2015) Efficient integration of synaptic events by NMDA receptors in three-dimensional neuropil. *Biophys J* 108:2457–2464.
17. Kim E, Owen B, Holmes WR, Grover LM (2012) Decreased afferent excitability contributes to synaptic depression during high-frequency stimulation in hippocampal area CA1. *J Neurophysiol* 108:1965–1976.
18. Tsodyks MV, Markram H (1997) The neural code between neocortical pyramidal neurons depends on neurotransmitter release probability. *Proc Natl Acad Sci USA* 94:719–723.
19. Crowley JJ, Carter AG, Regehr WG (2007) Fast vesicle replenishment and rapid recovery from desensitization at a single synaptic release site. *J Neurosci* 27:5448–5460.
20. Xie Y, et al. (2016) Resolution of high-frequency mesoscale intracortical maps using the genetically encoded glutamate sensor iGluSnFR. *J Neurosci* 36:1261–1272.
21. Clements JD, Lester RA, Tong G, Jahr CE, Westbrook GL (1992) The time course of glutamate in the synaptic cleft. *Science* 258:1498–1501.
22. Scimemi A, Beato M (2009) Determining the neurotransmitter concentration profile at active synapses. *Mol Neurobiol* 40:289–306.
23. Zheng K, et al. (2017) Nanoscale diffusion in the synaptic cleft and beyond measured with time-resolved fluorescence anisotropy imaging. *Sci Rep* 7:42022.
24. Compans B, Choquet D, Hosy E (2016) Review on the role of AMPA receptor nano-organization and dynamic in the properties of synaptic transmission. *Neurophotonics* 3:041811.
25. Carbone AL, Plested AJ (2016) Superactivation of AMPA receptors by auxiliary proteins. *Nat Commun* 7:10178.
26. Brager DH, Cai X, Thompson SM (2003) Activity-dependent activation of presynaptic protein kinase C mediates post-tetanic potentiation. *Nat Neurosci* 6:551–552.
27. Walklate J, Geeves MA (2015) Temperature manifold for a stopped-flow machine to allow measurements from -10 to +40°C. *Anal Biochem* 476:11–16.
28. Gee CE, Ohmert I, Wiegert JS, Oertner TG (2017) Preparation of slice cultures from rodent hippocampus. *Cold Spring Harb Protoc* 2017:pdb.prot094888.
29. Wiegert JS, Gee CE, Oertner TG (2017) Single-cell electroporation of neurons. *Cold Spring Harb Protoc* 2017:pdb.top089714.